

End superconductivity and three critical temperatures in Fibonacci quasicrystals

Quanyong Zhu,¹ Guo-Qiao Zha,² A. A. Shanenko,^{3,4} and Yajiang Chen^{5,*}

¹*School of Mathematics and Computer Science, Lishui University, 323000 Lishui, China*

²*Physics Department, Shanghai Key Laboratory of High Temperature Superconductors, Shanghai University, Shanghai 200444, China*

³*HSE University, 101000 Moscow, Russia*

⁴*Moscow Center for Advanced Studies, Kulakova str. 20, Moscow 123592, Russia*

⁵*Zhejiang Key Laboratory of Quantum State Control and Optical Field Manipulation, Department of Physics, Zhejiang Sci-Tech University, 310018 Hangzhou, China*

(Dated: October 7, 2024)

Recently, the superconducting properties of Fibonacci quasicrystals have attracted considerable attention. By numerically solving the self-consistent Bogoliubov-de Gennes equations for a Fibonacci chain under superconducting proximity, we find that the system exhibits universal end superconductivity, where the pair potential at the chain ends can persist at higher temperatures compared to the bulk critical temperature (T_{cb}) of the condensate in the chain center. Furthermore, our study reveals two distinct critical temperatures at the left end (T_{cL}) and right end (T_{cR}), governing the superconducting condensate at the chain ends. This complex behavior arises from the competition between topological bound states and critical states, a characteristic of quasicrystals. Due to the geometric configuration of Fibonacci chain approximants, T_{cL} and T_{cb} are independent of the Fibonacci sequence number n , while T_{cR} significantly depends on the parity of n . With the chosen parameters, the maximal enhancement of T_{cR} occurs for even n , reaching up to 50% relative to T_{cb} , while T_{cL} can increase by up to 23%. Our study sheds light on the phenomenon of end superconductivity in Fibonacci quasicrystals, pointing to alternative pathways for discovering materials with higher superconducting critical temperatures.

I. INTRODUCTION

The Fibonacci chain has attracted great attention since the discovery of three-dimensional icosahedral quasicrystals [1, 2] and the realization of GaAs-AlAs heterostructures with alternating layers arranged in a Fibonacci sequence [3]. The breakdown of translational invariance in the Fibonacci chain and other quasicrystals leads to multifractal energy spectra with critical states [4–14]. These electronic states are distinct from both the extended states in periodic solids and the localized states in strongly disordered solids, being, so to speak, “in-between” [9], a characteristic highlighted by the term “critical”. Another important property of the Fibonacci chains is the presence of the topologically protected bound states [15–17] inherited from the parent crystals (e.g., a 2D square lattice) [18]. In general, Fibonacci quasicrystals exhibit a plethora of unusual phenomena. To name a few, in addition to the critical and topological bound states, one can mention the many-body localization [19], the hyperuniform states [20, 21], reentrant phenomena in the presence of disorder [22, 23], etc.

Superconducting properties have also been intensively studied in Fibonacci chains [8, 9, 24–28]. In particular, for a Fibonacci chain deposited on an s -wave superconductor, a disordered gap equation demonstrates that superconductivity can be enhanced by increasing disorder strength due to the overlap of critical states [25]. For a normal Fibonacci chain connecting s -wave supercon-

ductors, the self-consistent Bogoliubov-de Gennes (BdG) formalism shows that topological bound states contribute to superconductivity at each site [24]. In this case, the pair potential (order parameter) exhibits significant spatial variations with a power-law decay toward the center of the chain, induced by the multifractal energy spectrum and critical states [8, 9]. In contrast, for an s -wave superconducting Fibonacci chain [26], the spatial oscillations of the pair potential persist throughout the entire chain and are self-similar; however, the superconducting gap in the local density of states remains uniform across all sites. Based on these results, it has been claimed [26] that as the temperature increases, the superconducting condensate disappears simultaneously at all sites, indicating a unique critical temperature for the entire Fibonacci chain.

However, recent results obtained for an attractive Hubbard model with the s -wave pairing and uniform hopping [29–35] have revealed that the superconducting condensate near the system boundaries (at the chain ends in the one-dimensional case) can persist at temperatures higher than the bulk critical temperature T_{cb} . This effect, below referred to as the *end superconductivity*, stems from the constructive interference of itinerant quasiparticles, which are not localized near the boundaries but are instead spread throughout the entire system. Moreover, topological bound states can also contribute and further complicate the effect, as revealed for proximitized topological insulators within the Su-Schrieffer-Heeger model [36]. Thus, one can expect that the end superconductivity should manifest in the Fibonacci chain - a phenomenon that has been overlooked until now.

* yjchen@zstu.edu.cn

In this work, by numerically solving the self-consistent BdG equations, we investigate the end superconductivity in a proximitized Fibonacci chain positioned on top of an s -wave superconductor. The proximity of a massive superconductor remedies severe one-dimensional fluctuations and justifies the use of the mean-field treatment [37–39]. In addition, the one-dimensional Fibonacci chain is a reasonable simplification of the three-dimensional Fibonacci quasicrystal for sufficiently small in-plane hopping amplitudes [26], which also justifies the BdG equations. Our study demonstrates that, due to the competition between the critical and topological bound states, the system exhibits distinct left-end (T_{cL}) and right-end (T_{cR}) critical temperatures, which differ from the critical temperature at the chain center (T_{cb}) and, importantly, can be significantly higher.

The paper is organized as follows. The BdG equations for a Fibonacci chain with s -wave pairing are outlined in Sec. II, along with some details of the numerical algorithm. The results are discussed in Sec. III, which is divided into three subsections. In Section III A we investigate the pair potential $\Delta(i)$ together with its single-species quasiparticle contributions. The three critical temperatures (T_{cR} , T_{cL} and T_{cb}) are considered in Sec. III B. Finally, Sec. III C investigates how the three critical temperatures depend on microscopic parameters, such as the chain length and hopping amplitudes. Concluding remarks are given in Sec. IV.

II. THEORETICAL FORMALISM

To numerically investigate the end superconductivity in a Fibonacci chain positioned on top of an s -wave superconductor, we consider finite approximants S_n of the Fibonacci chain, which is obtained when the sequence number n approaches infinity [40]. Each finite approximant S_n contains two sorts of sites (A and B). Its length is equal to the Fibonacci number F_n , where $\{F_1, F_2, F_3, F_4, F_5, \dots\} = \{1, 1, 2, 3, 5, \dots\}$. Following the Fibonacci sequence rule, the approximant S_n is the concatenation of S_{n-1} and S_{n-2} , i.e., $S_n = [S_{n-1}, S_{n-2}]$, where S_1 and S_2 are given by $S_1 = [B]$ and $S_2 = [A]$, see Refs. 40 and 41.

In our study we utilize the well-known nearest-neighbor tight-binding model. The superconductivity proximity effect is described [42] by adding the attraction Hubbard term. Then, the corresponding grand-canonical Hamiltonian reads [33, 43, 45, 46]

$$\mathcal{H} - \mu \mathcal{N}_e = - \sum_{ij} t_{\langle ij \rangle} c_{i\sigma}^\dagger c_{j\sigma} - \sum_{i\sigma} \mu n_{i\sigma} - g \sum_i n_{i\uparrow} n_{i\downarrow}, \quad (1)$$

where μ is the chemical potential, $g > 0$ is the on-site attraction coupling, and \mathcal{N}_e is the electron number operator $\mathcal{N}_e = \sum_{i\sigma} n_{i\sigma} = \sum_{i\sigma} c_{i\sigma}^\dagger c_{i\sigma}$, with $c_{i\sigma}^\dagger$ and $c_{i\sigma}$ the creation and annihilation operators of an electron at site i with spin $\sigma = \uparrow, \downarrow$. The summation is over sites $i, j = 1$ to F_n .

There are two variants of the Fibonacci chain model: the off-diagonal version, with the quasiperiodic hopping amplitude, and the diagonal model with on-site energies arranged according to the Fibonacci rule, e.g., see Ref. 25. These variants have similar results. In our study, we apply the off-diagonal Fibonacci model [25, 40, 47, 48]. The nearest-neighboring hopping amplitude $t_{\langle ij \rangle}$ is set to t_A between two A -sites, and t_B between A - and B -sites. Notice that two B -sites cannot be the nearest neighbors in the Fibonacci approximants.

Within the mean-field approximation, we obtain the effective Hamiltonian [43]

$$H_{\text{eff}} = - \sum_{ij\delta} (t_{\langle ij \rangle} + \mu \delta_{ij}) c_{i\sigma}^\dagger c_{j\sigma} + \sum_i [\Delta(i) c_{i\uparrow}^\dagger c_{i\downarrow}^\dagger + \Delta^*(i) c_{i\downarrow} c_{i\uparrow}], \quad (2)$$

where $\Delta(i)$ is the pair potential, and δ_{ij} is the Kronecker delta function. The Hartree-Fock potential is ignored in Eq. (2) because it merely shifts the chemical potential and produces a minor effect on the superconducting properties [35, 49]. Diagonalization of the effective Hamiltonian given by Eq. (2) yields the BdG equations [30, 32, 43, 46]

$$\sum_j -(t_{\langle ij \rangle} + \mu \delta_{ij}) u_\alpha(j) + \Delta(i) v_\alpha(i) = \varepsilon_\alpha u_\alpha(i), \quad (3a)$$

$$\Delta^*(i) u_\alpha(i) + \sum_j (t_{\langle ij \rangle} + \mu \delta_{ij}) v_\alpha(j) = \varepsilon_\alpha v_\alpha(i), \quad (3b)$$

with ε_α , $u_\alpha(i)$, and $v_\alpha(i)$ being the energy, electron- and hole-like wavefunctions of the quasiparticle with the quantum number α . For convenience, we arrange all the positive-energy quasiparticles in the energy ascending order so that the quantum number α represents the ordering number of the quasiparticle energy, i.e., the larger is α , the higher is ε_α . The open boundary conditions are applied to the quasiparticle wavefunctions: $u_\alpha(i)$ and $v_\alpha(i)$ are set to 0 at $i = 0$ and $i = F_n + 1$.

The BdG equations given by Eqs. (3) are solved in a self-consistent manner, together with the self-consistency condition

$$\Delta(i) = g \sum_{\varepsilon_\alpha \geq 0} u_\alpha(i) v_\alpha^*(i) (1 - 2f_\alpha), \quad (4)$$

with $f_\alpha = f(\varepsilon_\alpha)$ being the Fermi-Dirac distribution. The above sum runs over the physical states with $\varepsilon_\alpha \geq 0$. Moreover, the chemical potential μ in Eqs. (3) is determined by the average electron-filling level $\bar{n}_e = \sum_i n_e(i) / F_n$, with $n_e(i)$ being the spatial electron distribution of the form

$$n_e(i) = 2 \sum_\alpha [f_\alpha |u_\alpha(i)|^2 + (1 - f_\alpha) |v_\alpha(i)|^2]. \quad (5)$$

In our calculations, we employ the standard self-consistent numerical routine. First, we construct the

BdG equations with initial guessing values of μ and $\Delta(i)$. Second, ε_α , $u_\alpha(i)$ and $v_\alpha(i)$ are obtained by solving Eqs. (3). Then, we get new values for $\Delta(i)$ and μ by using Eqs. (4) and (5). These values are utilized to get the corresponding BdG equations, and the numerical procedure is repeated until convergence according to a chosen criterion. In our study, the iterative procedure is completed when an accuracy of about 10^{-10} is reached for both quantities $\Delta(i)$ and μ .

Below, the coupling g , the hopping parameter t_A , the chemical potential μ , the quasiparticle energy ε_α , and the pair potential $\Delta(i)$, are given in units of t_B while the temperature T is in units of t_B/k_B , with k_B the Boltzmann constant. In this study we adopt $g = 2$, which is common choice in literature [31, 33, 36, 46, 50]. The chain is considered in the half-filling regime. It is important to note that our qualitative conclusions are not sensitive to the choice of microscopic parameters.

III. RESULTS AND DISCUSSIONS

A. Pair potential and end superconductivity

Figure 1 illustrates typical spatial distributions of the pair potential $\Delta(i)$ calculated at $T = 0, 0.2, 0.233,$ and 0.245 for the Fibonacci chain approximant $S_{n=12}$ with $t_A = 0.8$. As is seen in panels (a) and (b), at $T = 0$ and 0.2 , $\Delta(i)$ shows remarkable fractal-like behavior inside the chain, which is fundamentally related to the multifractal critical character of the single-electron states in the Fibonacci quasicrystal [48]. At the chain ends (for $i = 1$ and F_n), we find that the local pair potential $\Delta(1)$ is much larger than $\Delta(F_n)$, i.e. the system exhibits significantly asymmetric condensate distribution. This feature is a consequence of the difference in the site configurations near the left and right chain ends: for $S_{n=12}$, we obtain the site sequence $[ABAABA\dots AABAAB]$.

When further increasing T up to 0.223 , see Fig. 1(c), the fractal-like pattern of the pair-potential oscillations disappears together with the condensate inside the chain. However, $\Delta(i)$ remains finite near the chain ends so that local maxima of $\Delta(i)$ occur at $i = 1$ and F_n with $\Delta(1) = 0.41$ and $\Delta(F_n) = 0.27$. Such asymmetric end superconductivity is even more significant at $T = 0.245$, as seen in Fig. 1(d). Here $\Delta(F_n)$ vanishes while $\Delta(1)$ is about 0.30 , i.e., the superconducting condensate only survives near the left end at $T = 0.245$. Thus, we find that the Fibonacci chain approximant exhibits clear signatures of the end superconductivity in agreement with the so-called interference-induced end superconductivity in the topological-trivial attractive Hubbard chain [31–33, 35]. However, the important difference is that in the latter case, the end superconductivity is characterized by the symmetric distribution of the Cooper-pair condensate with respect to the chain center.

To go into more detail, we investigate the single-species

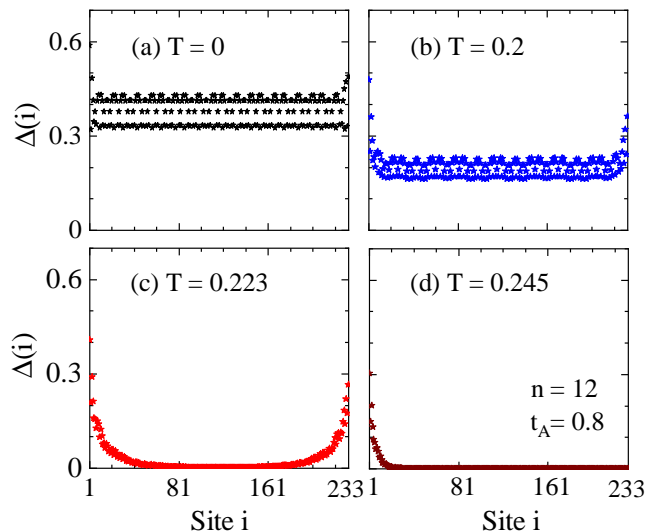


FIG. 1. The pair potential $\Delta(i)$ versus the site index at $T = 0, 0.2, 0.223,$ and 0.245 with $t_A = 0.8$ for the Fibonacci approximant $S_{n=12}$ with the total number of sites $F_n = 233$.

contribution of quasiparticles to $\Delta(i)$ given by [32, 33, 35]

$$\Delta_\alpha(i) = g u_\alpha(i) v_\alpha^*(i) (1 - 2f_\alpha). \quad (6)$$

Figures 2(a-b, e-f) show $\Delta_\alpha(i = 1, F_n)$ as a function of the quantum number α for the approximant $S_{n=12}$ with $t_A = 0.8$ at $T = 0.223$ and 0.245 , respectively. For comparison, the bulk single-quasiparticle contribution to the pair potential $\Delta_\alpha(\text{bulk})$ is given in Fig. 2(c, g) for the same temperatures. $\Delta_\alpha(\text{bulk})$ is defined as the average of $\Delta_\alpha(i)$ over the range $0.4F_n \leq i \leq 0.6F_n$. The corresponding quasiparticle energy spectrum, ε_α , is shown for the two temperatures mentioned above in Fig. 2(d, h), where the insets represent zoom-ins near zero energy. Only physical quasiparticles (i.e., $\varepsilon_\alpha \geq 0$) are considered according to Eq. (4). One can find that there are no zero-energy quasiparticles, which means that the Fibonacci chain with the s -wave pair correlations does not exhibit topological superconductivity.

From Figs. 2(a, b, e, f), we find that quasiparticles with odd (even) α give positive (negative) contributions to $\Delta(i = 1, F_n)$ at $T = 0.223$ and 0.245 . With increasing α , pronounced oscillations of $\Delta_\alpha(i = 1, F_n)$ around zero for both temperatures are due to rapid sign variations of $u_\alpha(i)$ and $v_\alpha(i)$ at the chain ends, which is similar to the results of the one-dimensional attractive Hubbard model with the uniform hopping amplitude [51]. Higher-energy quasiparticles with $\varepsilon_\alpha > 1.71$ produce almost negligible contributions to the superconducting condensate at the chain ends. This is not the case for the bulk pair potential: one can see the spatial profiles of $\Delta_\alpha(\text{bulk})$ at $T = 0.233$ and 0.245 in Figs. 2(c, g). Here the contributions of higher-energy quasiparticles with $\varepsilon_\alpha > 1.71$ are more significant as compared to the chain ends.

One can see from Figs. 2(c, g) that the positive and negative contributions to Δ_{bulk} are the same for both

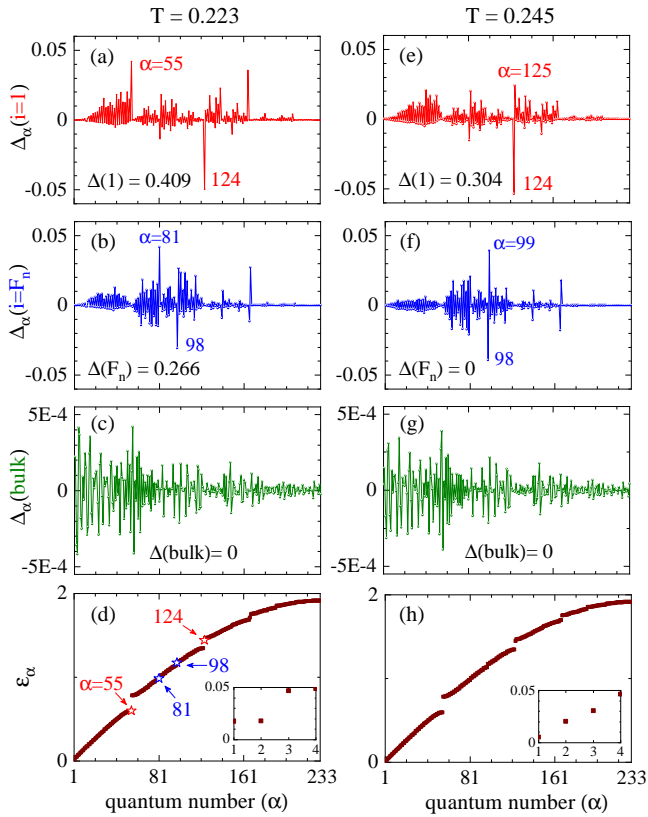


FIG. 2. (a-c, e-g) Single-species quasiparticle contribution $\Delta_\alpha(i)$ as a function of the quantum number α at $i = 1$ (red), $i = F_n$ (blue) and in the chain center (green) for $T = 0.223$ and 0.245 . (d, h) The quasiparticle energy spectrum ϵ_α at $T = 0.223$ and 0.245 , respectively. The values of $\Delta(i = 1, F_n, \text{bulk})$ and $\Delta_\alpha(\text{bulk})$ are marked, where $\Delta(\text{bulk})$ and $\Delta_\alpha(\text{bulk})$ are the relevant averages over the region of $0.4F_n \leq i \leq 0.6F_n$. In panels (d, h) the zoom-in plots around zero energy are shown. The results are calculated for the approximant $S_{n=12}$ with $t_A = 0.8$.

highlighted temperatures. Indeed, the positive and negative parts of the oscillation pattern of Δ_α are nearly mirror images of each other. This is a direct consequence of the fact that the superconducting condensate disappears in the chain center at $T = 0.223$ and 0.245 . A similar α -distribution of $\Delta_\alpha(F_n)$ is seen in Fig. 2(f), as $\Delta(i = F_n) = 0$ at $T = 0.245$. However, the positive parts in the oscillation patterns of Figs. 2(a, b, e) are more prominent than the negative parts, which leads to asymmetrical oscillations. This is related to the fact that $\Delta(1) = 0.409$ and $\Delta(F_n) = 0.266$ at $T = 0.233$, and $\Delta(1) = 0.304$ at $T = 0.245$. More specifically, at $T = 0.223$, the maximal and minimal contributions at the left end are $\Delta_{55}(1) = 0.103\Delta(1)$ and $\Delta_{124}(1) = -0.121\Delta(1)$. For the right end the maximal and minimal inputs are $\Delta_{81}(1) = 0.157\Delta(1)$ and $\Delta_{98}(1) = -0.116\Delta(1)$, respectively. At $T = 0.245$ in Fig. 2(e), the maximal and minimal contributions are $\Delta_{124}(1) = -0.176\Delta(1)$ and $\Delta_{125}(1) = 0.079\Delta(1)$.

The energies of the quasiparticles with $\alpha = 55, 81, 98$ and 124 are highlighted in the quasiparticle spectrum shown in Fig. 2(d). One can see that the quasiparticle energies for $\alpha = 55$ and 124 are at the band ends near substantial energy gaps. The single-electron states related to these quasiparticles are topological bound states of the normal Fibonacci chain with the energies located between bands [40]. In this work, the corresponding quasiparticles are referred to as *topological bound quasiparticles*. They are similar to the quasiparticles corresponding to the topological bound states in a proximitized Su-Schrieffer-Heeger chain [35]. In contrast, the states with $\alpha = 81$ and 98 are also topological bound quasiparticles but their energies are located near smaller band gaps not visible in the figure.

Figures 3(a-d, f-i) demonstrate spatial profiles of $\Delta_\alpha(i)$ and the probability density distribution $|u_\alpha(i)|^2 + |v_\alpha(i)|^2$ for the topological bound quasiparticles with $\alpha = 55$ (a, f), 124 (b, g), 81 (c, h), and 98 (d, i) at $T = 0.223$. The calculations are done for the same Fibonacci approximant $S_{n=12}$ with $t_A = 0.8$. In panels (a) and (b), both $\Delta_{55}(i)$ and $\Delta_{124}(i)$ exhibit pronounced rapid oscillations near the left end ($i = 1$) while vanishing at the right end ($i = F_n$). The decay spatial lengths for $\Delta_{55}(i)$ is much larger than that of $\Delta_{124}(i)$. Similarly, the probability density distributions given in Fig. 3(f) are pronounced near the left end while they drop to zero at the right end. The spatial localization of the state $\alpha = 124$ is much more significant as compared to that of $\alpha = 55$. In turn, for $\alpha = 81$ and 98 , both $\Delta_\alpha(i)$ in Figs. 3(c, d) and $|u_\alpha(i)|^2 + |v_\alpha(i)|^2$ in Figs. 3(h, i) exhibit rapid significant oscillations near the right end, $i = F_n$, while vanishing at the left end. Both states have nearly the same localization length. It is much larger than that of the state with $\alpha = 124$ and close to the localization length of the quasiparticles with $\alpha = 55$.

In Figs. 3(e, j), $\Delta_\alpha(i)$ and $|u_\alpha(i)|^2 + |v_\alpha(i)|^2$ are given versus the site index i for the quasiparticle state with $\alpha = 35$, representing the so-called critical single-electron states responsible for the fractal-like behavior of the pair potential inside the chain, see, e.g., Refs. [7–10]. Below, this kind of quasiparticles is referred to as *critical quasiparticles*. One can see, that contrary to the results for the topological bound quasiparticles, the oscillations in $\Delta_{35}(i)$ and $|u_{35}(i)|^2 + |v_{35}(i)|^2$ spread throughout the entire chain. For example, we obtain $\Delta_{35}(1) = 0.012$ and $\Delta_{35}(F_n) = 0.0067$. In addition, the probability density distribution of these quasiparticles has a clear multifractal character [52].

Now we focus on $T = 0.245$. The corresponding examples of $\Delta_\alpha(i)$ and $|u_\alpha(i)|^2 + |v_\alpha(i)|^2$ are shown as functions of the site number i in Fig. 4 for the topological bound quasiparticles with $\alpha = 124$ (a, f), 125 (b, g), 98 (c, h), 99 (d, i), and for the critical quasiparticle state with $\alpha = 41$ (e, j). As previously, the results are calculated for $S_{n=12}$ with $t_A = 0.8$. One finds that at $T = 0.245$ the curves of $\Delta_\alpha(i)$ and $|u_\alpha(i)|^2 + |v_\alpha(i)|^2$ for $\alpha = 124$ and 98 are almost the same as those calculated at $T = 0.233$

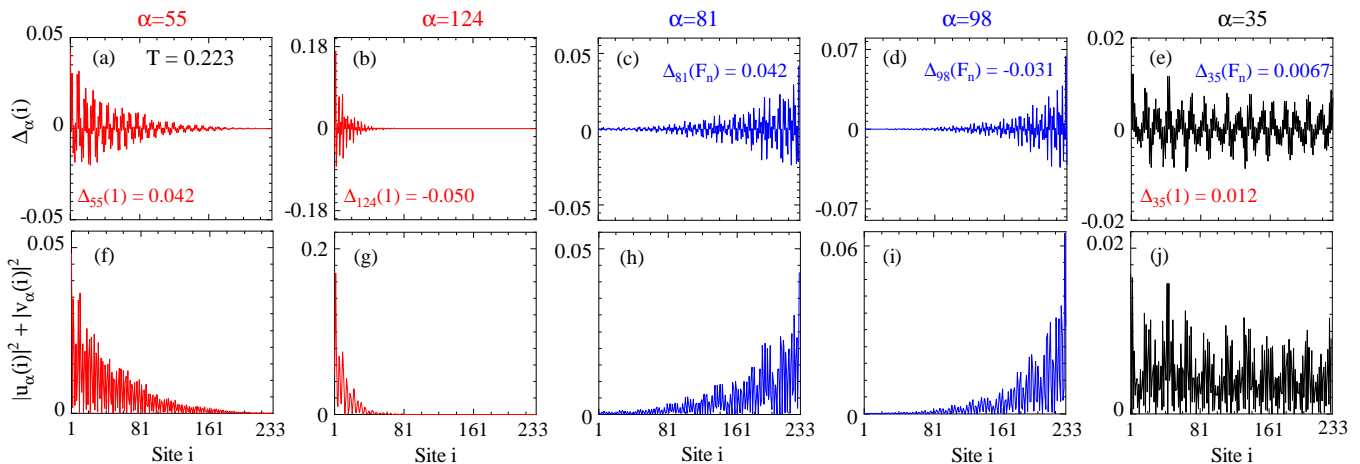


FIG. 3. (a-e) The spatial superconducting contributions $\Delta_\alpha(i)$ of typical topological bound quasiparticles with $\alpha = 55$ and 124 (in red), 81 and 98 (in blue), and the critical quasiparticle with $\alpha = 35$ (in black) for the chain S_n with $n = 12$ and $t_A = 0.8$ at $T = 0.233$; (f-j) The probability distributions $|u_\alpha(i)|^2 + |v_\alpha(i)|^2$ of quasiparticles with the same α 's.

and given in Figs. 3(b, c, g, h). The left-end localization length of $|u_{125}(i)|^2 + |v_{125}(i)|^2$ and $\Delta_{125}(i)$ in Figs. 4(b, g) is significantly larger than that of $\alpha = 124$ in Figs. 4(a, f). The spatial profiles of $\Delta_\alpha(i)$ and $|u_\alpha(i)|^2 + |v_\alpha(i)|^2$ for $\alpha = 98$ and 99 are similar in Figs. 4(c, h, d, e). However, the contributions of these quasiparticles to the right-end pair potential, i.e. $\Delta(i = F_n)$, are of opposite signs: $\Delta_{99}(F_n) = -\Delta_{98}(F_n) = 0.039$. This is certainly related to the fact that the right-end pair potential is zero at $T = 0.245$, as the superconducting condensate survives only at the left end of the chain.

The critical quasiparticle state with $\alpha = 41$ is spread throughout the whole chain, producing the end pair-potential contributions $\Delta_{41}(1) = 0.0208$ and $\Delta_{41}(F_n) = 0.0026$, which are comparable to those of the topological bound states. This is similar to the behavior of other critical quasiparticles, see the results for $T = 0.223$ in Figs. 3(e, j). However, for $T = 0.245$, we find that the superconducting condensate at $i = F_n$ is suppressed due to the destructive interference of the contributing states (together with bulk superconductivity) while the left-end pair potential remains enhanced due to their constructive interference.

Thus, similar to the previous results [31–34, 53] obtained for an ordinary one-dimensional attractive Hubbard model, we find that the interference of multiple quasiparticle states plays a significant role in the formation of an inhomogeneous condensate distribution with the pronounced end enhancements in the Fibonacci approximant $S_{n=12}$. This inhomogeneous superconductivity appears as a result of the complex interplay of the topological bound quasiparticles and non-localized critical quasiparticle states. This bears some similarity to the recent results for proximitized topological insulators within the Su-Schrieffer-Heeger model [35].

B. Three critical temperatures

Now, we address the problem of the critical superconductive temperatures in the Fibonacci chain approximants. As seen in Figs. 1(c, d), the superconductivity in the chain $S_{n=12}$ with $t_A = 0.8$ is essentially inhomogeneous, i.e., the end and bulk pair potentials $\Delta(i = 1, F_n, \text{bulk})$ drop to zero at different temperatures. As a result, one obtains distinct end and bulk critical temperatures, which is similar to the conclusions obtained for a one-dimensional attractive Hubbard model with uniform hopping in Refs. 31–34, and 53. Moreover, the pair potential at the left end of the chain in Fig. 1 persists at higher temperatures compared to the right end. In this way, we observe two distinct end critical temperatures: left (T_{cL}) and right (T_{cR}). Such a characteristic feature does not exist in the ordinary Hubbard model, see Refs. 31–34, and 53. In this section, we investigate how the bulk T_{cb} , T_{cL} , and T_{cR} are sensitive to the parameters n and t_A .

The T -dependent pair potential $\Delta(i)$ at $i = 1, F_n$ and inside (bulk) the chain $S_{n=12}$ is shown in Figs. 5(a-d) for $t_A = 0.8, 1, 1.2,$ and 2 with curves marked by triangles, spheres, and squares, respectively. To better understand the microscopic picture, Figs. 5(e-h) illustrate the corresponding single-species quasiparticle contribution $\Delta_\alpha(i)$ as a function of α at $T = 0$. In general, one can see that the T -dependent data for $\Delta(i)$ are similar to those of the conventional BCS theory [43].

From Figs. 5(a-d) one finds that $\Delta(i = 1, F_n, \text{bulk})$ and the critical temperatures T_{cR} , T_{cL} , and T_{cb} are very sensitive to t_A . In particular, at the case of $t_A = 0.8$ illustrated in Fig. 5(a), we obtain $T_{cL} > T_{cR} > T_{cb}$ with $T_{cL} = 0.27$, $T_{cR} = 0.243$ and $T_{cb} = 0.222$. This unusual end superconductivity (with the breakdown of the left-right symmetry) is determined by the competition between the topological bound and critical quasiparti-

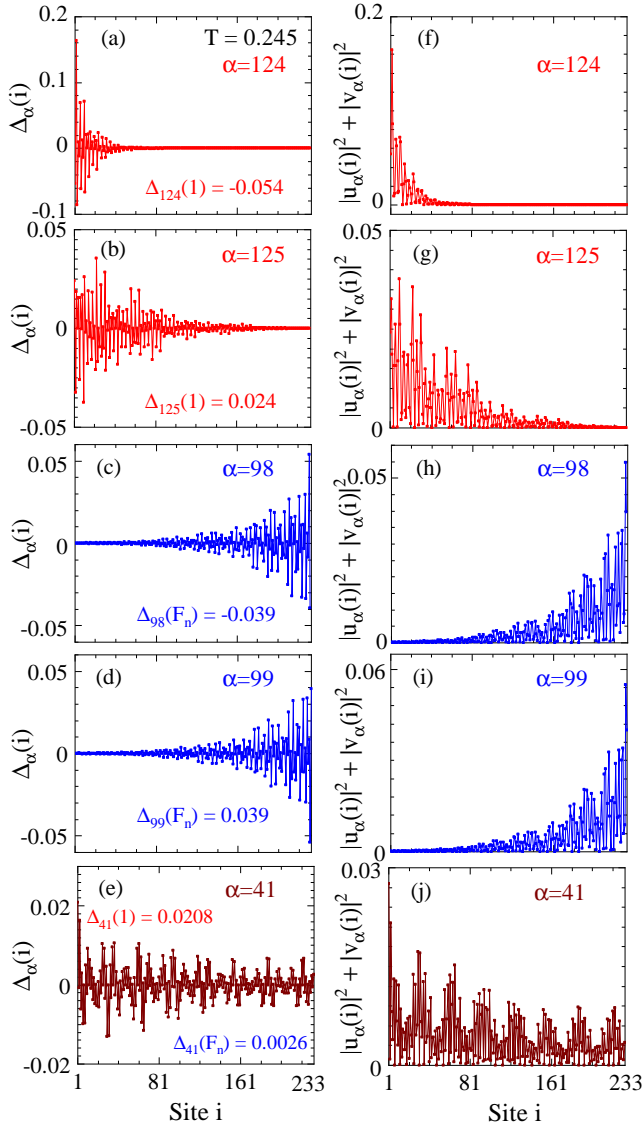


FIG. 4. The same as in Fig. 3, but for the topological bound quasiparticles of $\alpha = 124, 125, 98, 99$ and the critical quasiparticle of $\alpha = 41$ at $T = 0.245$.

cles, as discussed in the previous subsection. For $t_A = 1$, the system is reduced to the ordinary attractive Hubbard model without topological bound and critical states [32]. As a result, the left- and right-end pair potentials $\Delta(1)$ and $\Delta(F_n)$ become the same, and we arrive at the results obtained previously in Refs. 31 and 32. In this case, the constructive interference of the low-energy quasiparticles is responsible for the appearance of the left-right symmetric end superconductivity.

For $t_A = 1.2$, see Fig. 5(c), $\Delta(1)$ and T_{cL} are less than $\Delta(F_n)$ and T_{cR} , respectively. In this case, at $T = 0$, the quasiparticle contribution of $\alpha = 55$ predominates in the right-end pair potential: $\Delta_{55}(F_n) = 0.32\Delta(F_n)$. At the left end, we have two notable inputs to the pair potential. They are related to the quasiparticles with $\alpha = 56$ and

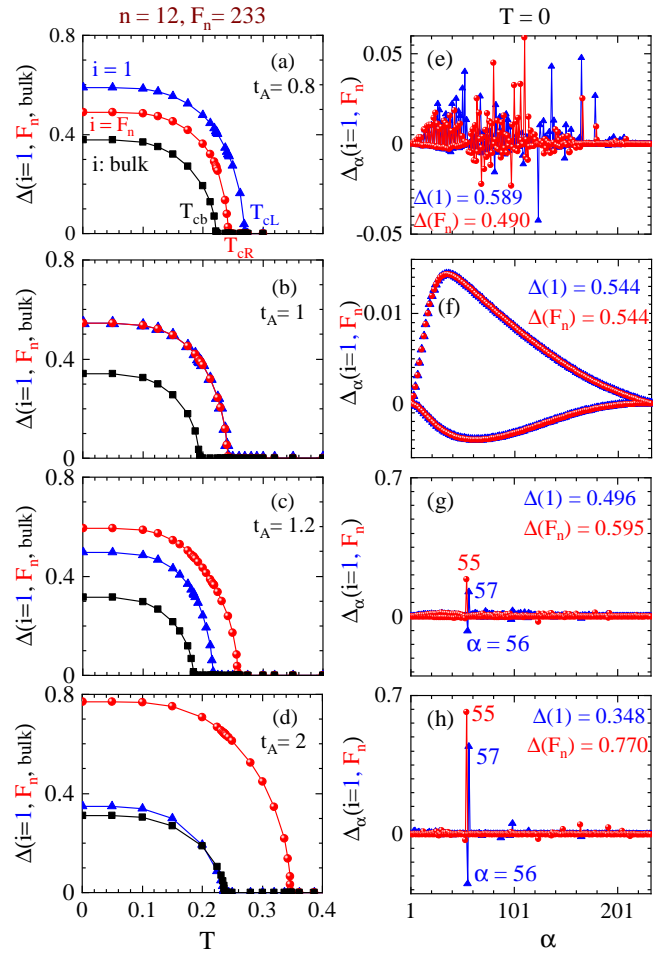


FIG. 5. (a-d) T -dependent pair potentials $\Delta(i)$ at the ends $i = 1$ (in blue), F_n (in red) and in bulk (in black) of the chain approximant $S_{n=12}$ for $t_A = 0.8, 1, 1.2$, and 2 . The critical temperatures T_{cL}, T_{cR} and T_{cb} are illustrated in panel (a), at which the corresponding local pair potentials drop to zero; (e-h) $\Delta_\alpha(i = 1, F_n)$ as functions of α for the same t_A at $T = 0$. The values of $\Delta(1)$ and $\Delta(F_n)$ are shown in these panels.

$\alpha = 57$. However, these inputs have opposite signs so that their sum is comparable with the contributions of other quasiparticles, see Fig. 5(g).

When t_A goes up to 2, see Fig. 5(d), one obtains $T_{cR} = 1.46T_{cL} = 0.348$ and $T_{cL} = T_{cb} = 0.238$. In this case, the left-end pair potential is nearly the same as the bulk pair potential. One can also see that at $T = 0$, the maximal contribution to the right-end pair potential comes from the quasiparticles with $\alpha = 55$. It reaches $0.8\Delta(F_n)$: the enhancement of the right-end superconductivity is mainly due to the topological bound states with $\alpha = 55$. For the left-end pair potential, there are two most important contributions from the quasiparticles with $\alpha = 56$ and $\alpha = 57$. They are of the opposite signs, i.e. $\Delta_{57}(1) = 1.27\Delta(1) = 0.442$ and $\Delta_{56}(1) = -0.72\Delta(1) = -0.249$. Most likely, the presence of such opposite contributions is responsible for the

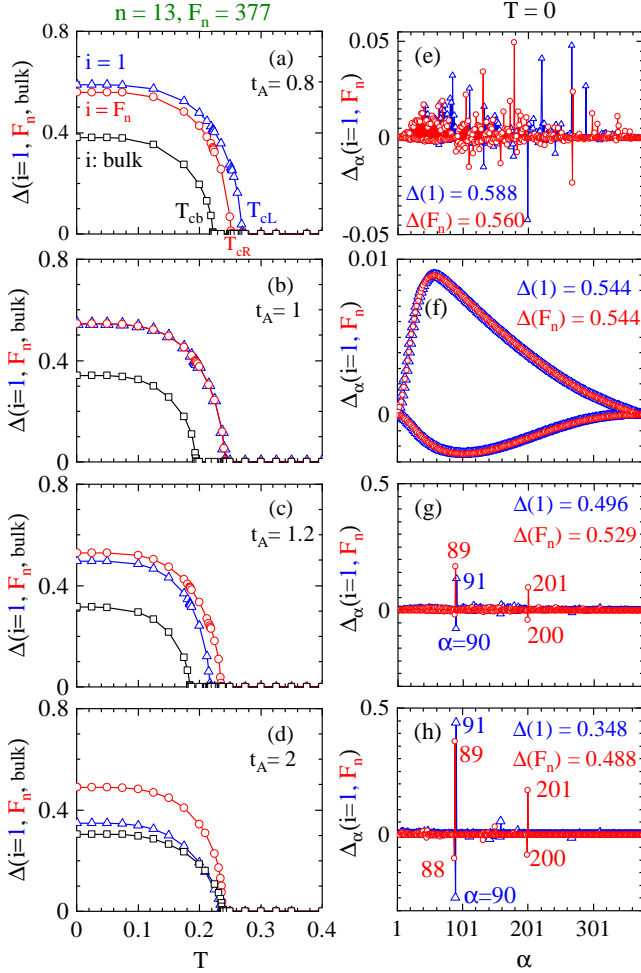


FIG. 6. The same as in Fig. 5 but for the Fibonacci approximant $S_{n=13}$ with $F_n = 377$.

disappearance of the left-end enhancement of superconductivity in the chain of interest.

Now we change the Fibonacci approximant and consider the system with $n = 13$ and $F_n = 377$. We plot $\Delta(i = 1, F_n, \text{bulk})$ as functions of T in Figs. 6(a-d), and $\Delta_\alpha(i = 1, F_n, \text{bulk})$ as functions of α in Figs. 6(e-h) at $T = 0$ for $t_A = 0.8, 1, 1.2$ and 2 . The curves of $\Delta(i = 1, \text{bulk})$ in Figs. 6(a-d) are the same as those in Figs. 5(a-d). It means that T_{cL} and T_{cb} for $n = 13$ are equal to the corresponding critical temperatures of $S_{n=12}$ (of course, for the corresponding values of t_A). Based on these results, one can expect that the quantities $\Delta(i = 1, \text{bulk})$, T_{cL} and T_{cb} are independent on n . This n -invariance is present because the site configuration near the left end does not change with n for a sufficiently long chain. In turn, the arrangement of the chain sites in the domain $[0.4F_n, 0.6F_n]$, used to define $\Delta(\text{bulk})$, is repeated for all n under the construction routine of the Fibonacci chain. The latter also takes place for sufficiently large n . [Our study demonstrates that the finite size effects are negligible for $n \gtrsim 10$.] This is re-

flected in the n -invariance of our results for the left-end and bulk superconductive characteristics in Figs. 5 and 6. Here, one should not be confused with the different quantum numbers of the quasiparticles that produce the most significant contribution to $\Delta(1)$ for $n = 12$ and $n = 13$, see, e.g., Figs. 5(h) and 6(h). Indeed, in our numerical procedure, the quasiparticle states are enumerated in the energy ascending order and, so, quasiparticles with the same α do not represent the same states for different n .

When further comparing Figs. 5 and 6, one can see that contrary to the left-end and bulk characteristics, $\Delta(F_n)$ and T_{cR} are not n -invariant, being very sensitive to the choice of n . This is related to the fact that the site configurations at the right end of the approximants $S_{n=12}$ and $S_{n=13}$ are different: the last three sites for $n = 12$ are arranged as AAB while for $n = 13$ we have ABA . In particular, this difference results in a significant deviation of the right-end pair potential of $S_{n=13}$ from that of $S_{n=12}$, see panels (e, g, h) of Figs. 5 and 6. The most pronounced deviation occurs at $t_A = 2$, at which $T_{cR} = T_{cL}$ for $n = 13$ but $T_{cR} = 1.46T_{cL}$ at $n = 12$.

One can also see that for $n = 12$, the most significant input to the right-end pair potential $\Delta(F_n)$ comes from the quasiparticles with $\alpha = 55$ (here we discuss the results at $T = 0$). On the contrary, there are four states producing essential contributions to $\Delta(F_n)$ for $n = 13$: these are quasiparticles with $\alpha = 88, 89, 200$, and 201 . Moreover, these four states produce contributions of opposite signs, which can be related to the drop of T_{cR} down to T_{cb} .

C. Dependence of the critical temperatures on t_A and n

Here, we focus on a more systematic study of how the controlling parameters t_A and n affect T_{cR} , T_{cL} , and T_{cb} . In particular, Fig. 7 shows these critical temperatures as functions of t_A for $n = 10, \dots, 15$; the left (right) panels correspond to even (odd) n . T_{cR} and T_{cL} are given by curves with red circles and blue triangles, respectively. T_{cb} is shown by the black curves with squares. In all panels, the site configurations on the left (blue) and right (red) ends of the approximants S_n are highlighted.

In agreement with the discussion of Sec. III B, we find from Fig. 7 that T_{cb} (black curves marked by triangles) does not change with n (except of the case with $n = 10$, where the results are slightly shifted due to finite-size effects). One can see that the bulk critical temperature reaches its minimum $T_{cb} = 0.186$ at $t_A = 1.2$. This value of the hopping parameter is close to $t_A = 1$ of the ordinary attractive Hubbard model with the periodic chain. When t_A increases above $t_A = 1.2$ or decreases below this point, T_{cb} grows significantly, which agrees with the previous results of the disordered gap equation [25]. Notice that T_{cb} is also dependent on other parameters, e.g., the chemical potential μ and the coupling strength g [26]. However, investigations of these aspects are beyond the

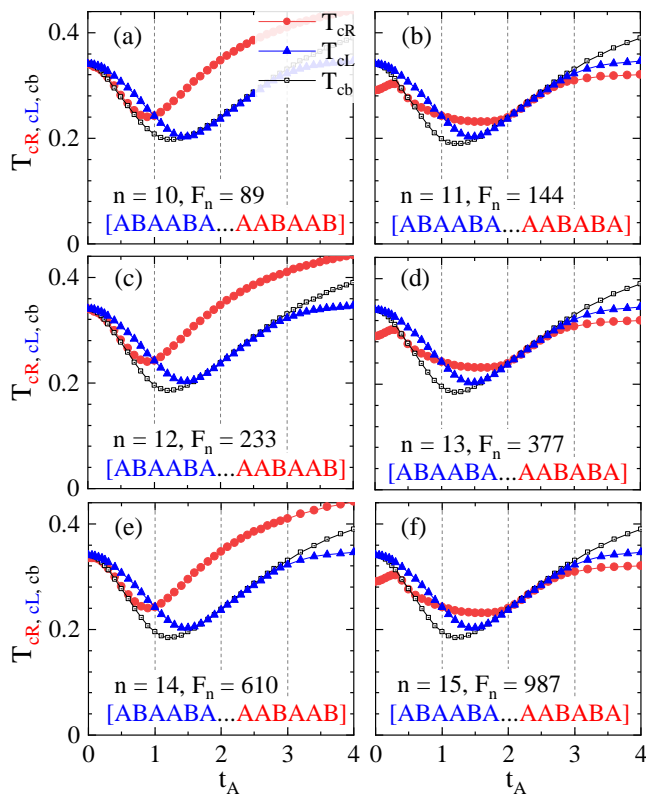


FIG. 7. The critical temperatures T_{cL} (in blue), T_{cR} (in red) and T_{cb} (in black) as functions of t_A for the approximants S_n with $n = 10, \dots, 15$ in panels (a-f), respectively. The left (right) panels are for the even (odd) n . Six site symbols close to the ends of the chains are marked in all panels.

scope of our work.

One can also see that T_{cL} (the blue curves with triangles) is independent of n in Fig. 7, which agrees with the results of Figs. 5 and 6. As explained in the last paragraph of Sec. III B, this is due to the same site configuration on the left end of the chains with different n . The first six sites at the left end for $n = 10, \dots, 15$ are the same and given by the sequence $ABAABA$ marked in blue in Figs. 7(a-f).

As is expected from Sec. III B, the right-end critical temperature exhibits significant variations with n . This is also seen in Figs. 7(a-f). Furthermore, one finds that the behavior of T_{cR} (red curves with circles) versus t_A strongly depends on the parity of n . This is certainly related to the fact that the first six sites on the right end of the chain are determined by this parity. We have $AABAAB$ for even n , see Figs. 7(a, c, e), while we obtain $AABABA$ for odd n , see Figs. 7(b, d, f). There are two important features different for even and odd values of n .

First, in the limit $t_A \rightarrow 0$, T_{cR} and T_{cL} calculated for an even n are nearly the same while for an odd n , T_{cR} is less than T_{cL} . This can be understood as follows. The chain is practically cut into short connected segments

when $t_A \rightarrow 0$, because the hopping between two neighboring A -sites is suppressed. The superconductivity in such segments is affected by quantum confinement for the condensate at both ends of any segment. As seen in Fig. 7, the nearly isolated segment on the left end of the chain is ABA for all n . In turn, the nearly isolated segment at the right end of the chain is AB for an even n and $ABABA$ for an odd n . When n is even, we compare the superconducting properties in ABA at the left end and AB at the right end. Both segments are characterized by the significant influence of confinement. Then, one can expect that the properties of the superconductive condensate confined in such segments are similar. In this case, our calculation yields almost the same T_{cL} and T_{cR} , see Figs. 7(a, c, e). When an odd n is chosen, we compare the superconducting properties of ABA at the left end and $ABABA$ at the right end. Here one can see that the confinement effects are weaker in the longer segment $ABABA$. This suggests that the condensate properties in ABA (left) and $ABABA$ (right) are different, and our numerical results demonstrate that T_{cL} differs from T_{cR} in Figs. 7(b, d, f).

The second difference between the results for even and odd values of n is as follows. For $t_A \geq 2$, T_{cR} for even n is higher than T_{cL} but for odd n , T_{cR} is equal or lower than T_{cL} . It is already known from the discussion of Figs. 5(d) and 6(d) that the enhancement of T_{cR} at $t_A \geq 2$ for even n comes from the predominating contribution of a single species of topological bound states to the right-end pair potential, see Fig. 5(h). On the contrary, for odd n , there are multiple contributions to $\Delta(i = F_n)$ from various topological bound states with opposite signs, see Fig. 6(h). This leads to a decrease in T_{cR} with respect to T_{cL} .

It is important to point out that T_{cL} and T_{cR} are not always larger than T_{cb} . Indeed, for odd n and $t_A \gtrsim 2.5$ both the left- and right-end critical temperatures are smaller than T_{cb} . The most pronounced enhancement of the end superconductivity in the Fibonacci chain approximant is observed at even n for $t_A \gtrsim 1$ at the right end.

Additional details can be found in Fig. 8, where the quantities $\tau_L = (T_{cL} - T_{cb})/T_{cb}$ and $\tau_R = (T_{cR} - T_{cb})/T_{cb}$ are given as functions of t_A for $n = 10, \dots, 15$. The curves with blue triangles correspond to τ_L while those with red circles represent τ_R . The left panels (a, c, e) are for even n values while the right ones are for odd n . Here, we clearly see that the left-end superconductivity is enhanced as compared to the bulk superconductivity only for $t_A \lesssim 1.5$. In this case, we have $\tau_L > 0$. The maximum enhancement of T_{cL} is obtained at $t_A = 1$, irrespective of a particular value of n . [We note that this maximum is slightly less pronounced for $n = 10$ due to the finite-size effects that disappear for larger values of n .] The regime of the right-end enhancement of superconductivity (with respect to bulk) takes place for $t_A > 0.5$ at even n , and for $0.5 < t_A < 1.5$ for odd n . The maximum of τ_R is about 50% at $t_A \approx 1.6$ for even n and about 25% at $t_A \approx 1.2$ for odd n . We find that the maximum of τ_R for

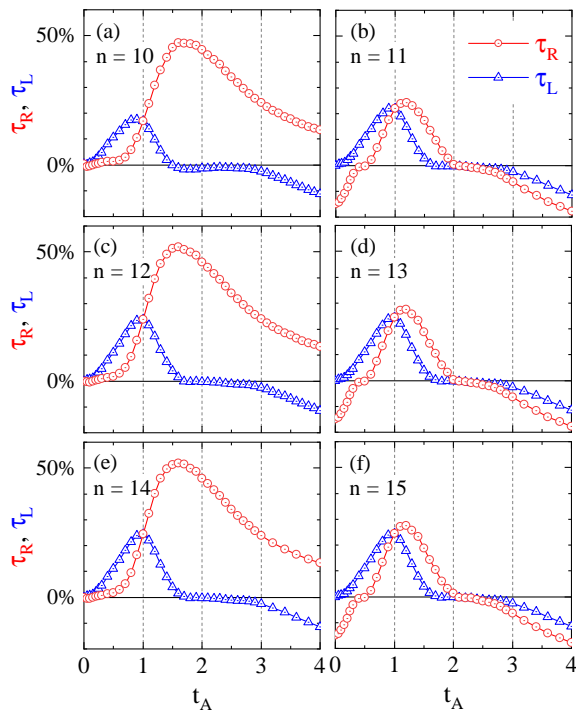


FIG. 8. The relative enhancement of the end critical temperatures $\tau_{R,L} = (T_{cR,cL} - T_{cb})/T_{cb}$ as functions of t_A for the Fibonacci approximants S_n with $n = 10, \dots, 15$. The black horizontal solid lines indicate zero.

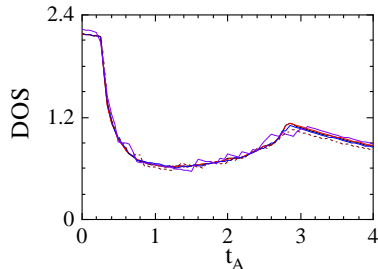


FIG. 9. Density of states (DOS) at $T = 0$ and $g = 0$, given by $\frac{dN}{F_n dE}|_{E=\mu}$ as a function of t_A in units of t_B^{-1} for $n = 10, \dots, 15$.

even n is twice as much as its maximum for odd n .

Finally, we study the impact of the density of states (DOS) on T_{cb} in the Fibonacci approximants. Figure 9 demonstrates the DOS, defined as $dN/(F_n dE)$ at $E = \mu$, with dN being the number of states in the energy interval dE around $E = \mu$. It is given as a function of t_A and calculated for $n = 10, \dots, 15$ at $T = 0$ and $g = 0$. As seen from Fig. 9, when increasing t_A , the DOS first drops to its minimum value of about 0.6 at $t_A \approx 1.2$. Then, when t_A exceeds 1.2, the DOS increases until it reaches its maximum of about 1.1 at $t_A \approx 2.8$. For $t_A > 2.8$, the DOS decreases linearly. Comparing these results with those for T_{cb} (the squared black curves) in Fig. 7, one concludes that T_{cb} follows the DOS in the region of $0 < t_A < 2.8$: the larger the DOS is, the higher the

critical temperature gets. This agrees with the textbook BCS picture [43, 54]. However, at $t_A > 2.8$, T_{cb} and the DOS exhibit opposite trends: T_{cb} increases with t_A while the DOS decreases. Our analysis suggests that this occurs due to the enhanced contribution of topological bound states, which is not governed by the standard BCS relation (unlike the contribution of the critical states).

IV. CONCLUSIONS

By numerically solving the self-consistent Bogoliubov-de Gennes equations, we have systematically investigated the end superconductivity in the Fibonacci approximants S_n with $n = 10, \dots, 15$, at the half filling and under the s -wave superconducting proximity. It has been found that the pair potential is significantly enhanced at the ends of the chain for the quasiperiodic strengths $t_A/t_B \approx 1-2$. The effect is induced by the complex interplay of the topological bound states and the constructive interference of the critical quasiparticles near the chain ends. Due to different configurations of the Fibonacci approximants at the left and right ends, we find different enhancements at the left and right ends. As a result, we obtain the system with the three distinct critical temperatures: the left and right end critical temperatures (T_{cL} and T_{cR}), and the bulk critical temperature (T_{cb}). In this case, when the temperature is increased, the system first becomes normal in the chain center and then at the chain ends.

Our numerical study shows that T_{cL} and T_{cb} are independent of the approximant sequence number $n > 10$. The relative enhancement of T_{cL} with respect to T_{cb} , i.e., $\tau_L = (T_{cL} - T_{cb})/T_{cb}$, reaches its maximum about 23% at $t_A/t_B \approx 1$. On the other hand, T_{cR} is sensitive to n . Its relative enhancement with respect to T_{cb} , i.e., $\tau_R = (T_{cR} - T_{cb})/T_{cb}$, can be notably larger than τ_L . In particular, for even n we find $\tau_R \approx 50\%$ at $t_A/t_B \approx 1.6$. For odd n we obtain $\tau_R \approx 20\%$ at $t_A/t_B \approx 1.2$.

When t_A/t_B exceeds 2, the both quantities τ_L and τ_R decrease with increasing t_A/t_B . This results in the suppression of the end superconductivity for $t_A/t_B \gtrsim 3-4$. In this case, when the temperature is increased, the system first becomes normal at the ends and then in the chain center. For $t_A/t_B \ll 1$ any signatures of the left-end superconductivity disappear irrespective of a particular value of n . However, the right-end superconductivity is still notably dependent on n . For even n , the system exhibits the only critical temperature while for odd n the right-end critical temperature is smaller than the bulk one.

Thus, this study sheds light on the complex properties of superconducting quasicrystals, demonstrating the presence of the three critical temperatures in the Fibonacci approximants. Our results may appeal to those interested in the physics of quasicrystals and emerging superconducting materials.

ACKNOWLEDGMENTS

This work was supported by the Science Foundation of Zhejiang Sci-Tech University (Grants No. 19062463-Y). A.A.S. thanks the Grant of Ministry of Science and

Higher Education of the Russian Federation No. 075-15-2024-632 for the support that helped to perform investigations of the end critical temperatures in the Fibonacci chain. Analysis of numerical data was partly supported by the HSE University Basic Research Program.

-
- [1] D. Shechtman, I. Blech, D. Gratias, and J. W. Cahn, Metallic Phase with Long-Range Orientational Order and No Translational Symmetry, *Phys. Rev. Lett.* **53**, 1951 (1984).
- [2] D. Levine and P. J. Steinhardt, Quasicrystals: A New Class of Ordered Structures, *Phys. Rev. Lett.* **53**, 2477 (1984).
- [3] R. Merlin, K. Bajema, R. Clarke, F. Y. Juang, and P. K. Bhattacharya, Quasiperiodic GaAs-AlAs Heterostructures, *Phys. Rev. Lett.* **55**, 1768 (1985).
- [4] A. Sütő, Singular continuous spectrum on a cantor set of zero Lebesgue measure for the Fibonacci Hamiltonian, *J. Stat. Phys.* **56**, 525 (1989).
- [5] J. Bellissard, B. Iochum, E. Scoppola, and D. Testard, Spectral properties of one dimensional quasi-crystals, *Commun. Math. Phys.* **125**, 527 (1989).
- [6] U. Grimm and M. Schreiber, Quasicrystals: Structure and Physical Properties (Springer, Heidelberg, 2003).
- [7] N. Macé, A. Jagannathan, and F. Piéchon, Fractal dimensions of wave functions and local spectral measures on the Fibonacci chain, *Phys. Rev. B* **93**, 205153 (2016).
- [8] G. Rai, S. Haas, and A. Jagannathan, Superconducting proximity effect and order parameter fluctuations in disordered and quasiperiodic systems, *Phys. Rev. B* **102**, 134211 (2020).
- [9] G. Rai, S. Haas, and A. Jagannathan, Induced superconducting pair correlations in a quasicrystal coupled to a BCS superconductor, *J. Phys.: Conf. Ser.* **1458**, 012013 (2020).
- [10] M. Reisner, Y. Tahmi, F. Piéchon, U. Kuhl, and F. Mortessagne, Experimental observation of multifractality in Fibonacci chains, *Phys. Rev. B* **108**, 064210 (2023).
- [11] P. G. Harper, Single Band Motion of Conduction Electrons in a Uniform Magnetic Field, *Proc. Phys. Soc. A* **68**, 874 (1955).
- [12] S. Aubry and G. André, Analyticity breaking and Anderson localization in incommensurate lattices, *Ann. Isr. Phys. Soc.* **13**, 18 (1980).
- [13] T. Lv, T.-C. Yi, L. Li, G. Sun, and W.-L. You, Quantum criticality and universality in the p-wave-paired Aubry-André-Harper model, *Phys. Rev. A* **105**, 013315 (2022).
- [14] T. Lv, Y.-B. Liu, T.-C. Yi, L. Li, M. Liu, and W.-L. You, Exploring unconventional quantum criticality in the p-wave-paired Aubry-André-Harper model, *Phys. Rev. B* **106**, 144205 (2022).
- [15] H. Huang and F. Liu, Quantum Spin Hall Effect and Spin Bott Index in a Quasicrystal Lattice, *Phys. Rev. Lett.* **121**, 126401 (2018).
- [16] H. Huang and F. Liu, Comparison of quantum spin Hall states in quasicrystals and crystals, *Phys. Rev. B* **100**, 085119 (2019).
- [17] M. Verbin, O. Zilberberg, Y. E. Kraus, Y. Lahini, and Y. Silberberg, Observation of Topological Phase Transitions in Photonic Quasicrystals, *Phys. Rev. Lett.* **110**, 076403 (2013).
- [18] M. Verbin, O. Zilberberg, Y. Lahini, Y. E. Kraus, and Y. Silberberg, Topological pumping over a photonic Fibonacci quasicrystal, *Phys. Rev. B* **91**, 064201 (2015).
- [19] N. Macé, N. Laflorencie, and F. Alet, Many-body localization in a quasiperiodic Fibonacci chain, *SciPost Phys.* **6**, 050 (2019).
- [20] S. Torquato, Hyperuniform states of matter, *Physics Reports* **745**, 1 (2018).
- [21] M. Baake and U. Grimm, Scaling of diffraction intensities near the origin: Some rigorous results, *J. Stat. Mech.* **2019**, 054003 (2019).
- [22] A. Jagannathan and M. Tarzia, Re-entrance and localization phenomena in disordered Fibonacci chains: Disorder induced crossover from critical states to Anderson localized states, *Eur. Phys. J. B* **93**, 46 (2020).
- [23] K. Singh, K. Saha, S. A. Parameswaran, and D. M. Weld, Fibonacci optical lattices for tunable quantum quasicrystals, *Phys. Rev. A* **92**, 063426 (2015).
- [24] G. Rai, S. Haas, and A. Jagannathan, Proximity effect in a superconductor-quasicrystal hybrid ring, *Phys. Rev. B* **100**, 165121 (2019).
- [25] M. Sun, T. Čadež, I. Yurkevich, and A. Andreanov, Enhancement of superconductivity in the Fibonacci chain, *Phys. Rev. B* **109**, 134504 (2024).
- [26] Y. Wang, G. Rai, C. Matsumura, A. Jagannathan, and S. Haas, Superconductivity in the Fibonacci chain, *Phys. Rev. B* **109**, 214507 (2024).
- [27] A. Kobińska, O. A. Awoga, M. Leijnse, T. Domański, P. Holmvall, and A. M. Black-Schaffer, Topological superconductivity in Fibonacci quasicrystals (2024), [arXiv:2405.12178 \[cond-mat\]](https://arxiv.org/abs/2405.12178).
- [28] A. Sandberg, O. A. Awoga, A. M. Black-Schaffer, and P. Holmvall, Josephson effect in a Fibonacci quasicrystal, *Phys. Rev. B* **110**, 104513 (2024).
- [29] M. Barkman, A. Samoilenka, and E. Babaev, Surface Pair-Density-Wave Superconducting and Superfluid States, *Phys. Rev. Lett.* **122**, 165302 (2019).
- [30] A. Samoilenka, M. Barkman, A. Benfenati, and E. Babaev, Pair-density-wave superconductivity of faces, edges, and vertices in systems with imbalanced fermions, *Phys. Rev. B* **101**, 054506 (2020).
- [31] M. D. Croitoru, A. A. Shanenko, Y. Chen, A. Vagov, and J. A. Aguiar, Microscopic description of surface superconductivity, *Phys. Rev. B* **102**, 054513 (2020).
- [32] Y. Bai, Y. Chen, M. D. Croitoru, A. A. Shanenko, X. Luo, and Y. Zhang, Interference-induced surface superconductivity: Enhancement by tuning the Debye energy, *Phys. Rev. B* **107**, 024510 (2023).
- [33] Y. Bai, L. Zhang, X. Luo, A. A. Shanenko, and Y. Chen, Tailoring of interference-induced surface superconductivity by an applied electric field, *Phys. Rev. B* **108**, 134506 (2023).
- [34] R. H. de Bragança, M. D. Croitoru, A. A. Shanenko,

- and J. A. Aguiar, Effect of Material-Dependent Boundaries on the Interference Induced Enhancement of the Surface Superconductivity Temperature, *J. Phys. Chem. Lett.* **14**, 5657 (2023).
- [35] Y. Chen, Q. Zhu, M. Zhang, X. Luo, and A. Shanenko, Surface superconductor-insulator transition: Reduction of the critical electric field by Hartree-Fock potential, *Physics Letters A* **494**, 129281 (2024).
- [36] Y. Chen, K.-J. Chen, J.-J. Zhu, and A. A. Shanenko, Emergence of surface superconductivity through interference in proximitized topological insulators, *Phys. Rev. B* **109**, 224514 (2024).
- [37] T. T. Saraiva, P. J. F. Cavalcanti, A. Vagov, A. S. Vasenko, A. Perali, L. Dell'Anna, and A. A. Shanenko, Multiband Material with a Quasi-1D Band as a Robust High-Temperature Superconductor, *Phys. Rev. Lett.* **125**, 217003 (2020).
- [38] T. T. Saraiva, L. I. Baturina, and A. A. Shanenko, Robust Superconductivity in Quasi-one-dimensional Multiband Materials, *J. Phys. Chem. Lett.* **12**, 11604 (2021).
- [39] A. A. Shanenko, T. T. Saraiva, A. Vagov, A. S. Vasenko, and A. Perali, Suppression of fluctuations in a two-band superconductor with a quasi-one-dimensional band, *Phys. Rev. B* **105**, 214527 (2022).
- [40] A. Jagannathan, The Fibonacci quasicrystal: Case study of hidden dimensions and multifractality, *Rev. Mod. Phys.* **93**, 045001 (2021).
- [41] W. M. Zheng, Global scaling properties of the spectrum for the Fibonacci chains, *Phys. Rev. A* **35**, 1467 (1987).
- [42] L. Fu and C. L. Kane, Superconducting Proximity Effect and Majorana Fermions at the Surface of a Topological Insulator, *Phys. Rev. Lett.* **100**, 096407 (2008).
- [43] P. G. de Gennes, *Superconductivity of Metals and Alloys* (Benjamin, New York, 1966).
- [44] M. Kohmoto, L. P. Kadanoff, and C. Tang, Localization Problem in One Dimension: Mapping and Escape, *Phys. Rev. Lett.* **50**, 1870 (1983).
- [45] S. Ostlund, R. Pandit, D. Rand, H. J. Schellnhuber, and E. D. Siggia, One-Dimensional Schrödinger Equation with an Almost Periodic Potential, *Phys. Rev. Lett.* **50**, 1873 (1983).
- [46] K. Tanaka and F. Marsiglio, Anderson prescription for surfaces and impurities, *Phys. Rev. B* **62**, 5345 (2000).
- [47] F. Piéchon, M. Benakli, and A. Jagannathan, Analytical Results for Scaling Properties of the Spectrum of the Fibonacci Chain, *Phys. Rev. Lett.* **74**, 5248 (1995).
- [48] A. Rüdinger and F. Piéchon, On the multifractal spectrum of the Fibonacci chain, *J. Phys. A: Math. Gen.* **31**, 155 (1998).
- [49] Y. Chen, M. D. Croitoru, A. A. Shanenko, and F. M. Peeters, Superconducting nanowires: Quantum confinement and spatially dependent Hartree-Fock potential, *J. Phys.: Condens. Matter* **21**, 435701 (2009).
- [50] S. G. Iodzik and A. Ptok, Quantum Phase Transition Induced by Magnetic Impurity: Triangular Lattice with On-Site Pairing Study, *J. Supercond. Nov. Magn.* **31**, 647 (2018).
- [51] L. Yin, Y. Bai, M. Zhang, A. A. Shanenko, and Y. Chen, Surface superconductor-insulator transition induced by electric field, *Phys. Rev. B* **108**, 054508 (2023).
- [52] M. Kohmoto, B. Sutherland, and C. Tang, Critical wave functions and a Cantor-set spectrum of a one-dimensional quasicrystal model, *Phys. Rev. B* **35**, 1020 (1987).
- [53] L. Chen, Y. Chen, W. Zhang, and S. Zhou, Non-gapless excitation and zero-bias fast oscillations in the LDOS of surface superconducting states, *Physica B: Condensed Matter* **646**, 414302 (2022).
- [54] J. B. Ketterson and S. N. Song, *Superconductivity* (Cambridge, 1999).